Numerical simulation of ballistic magnetoconductance and magnetic focusing in strained Si-SiGe cavities

Marco G. Pala
Dipartimento di Ingegneria dell'Informazione: Elettronica, Informatica, Telecomunicazioni, Università di Pisa
Giuseppe Iannaccone
Dipartimento di Ingegneria dell'Informazione: Elettronica, Informatica, Telecomunicazioni, Università di Pisa
Gilberto Curatola
Dipartimento di Ingegneria dell'Informazione: Elettronica, Informatica, Telecomunicazioni, Università di Pisa

M.G. Pala, G. Iannaccone, G. Curatola, *Numerical simulation of ballistic magnetoconductance and magnetic focusing in strained Si-SiGe cavities*, NANOTECHNOLOGY, **16**, pp.S206-S210 (2005).

Nanotechnology **16** (2005) S206–S210 doi:10.1088/0957-4484/16/5/013

Numerical simulation of ballistic magnetoconductance and magnetic focusing in strained Si–SiGe cavities

Marco G Pala[1,3], **Giuseppe Iannaccone**[1,2] **and Gilberto Curatola**[1]

[1] Dipartimento di Ingegneria dell'Informazione, Università degli Studi di Pisa, via Caruso, 56122 Pisa, Italy
[2] IEIIT-Consiglio Nazionale delle Ricerche, via Caruso, 56122 Pisa, Italy

E-mail: MP208580@chartreuse.cea.fr (M G Pala)

Received 12 September 2004, in final form 19 January 2005
Published 4 March 2005
Online at stacks.iop.org/Nano/16/S206

Abstract
We present numerical simulations of the transport properties of a ballistic cavity connected to two leads in the presence of a finite degree of decoherence. The cavity is obtained by realizing a 'quantum chicane', i.e., by shifting a short section of a quantum wire defined by etching on a SiGe heterostructure. We compare our results with experiments by Scappucci *et al* (2004 *Trends in Nanotechnology (Segovia, Spain, Sept. 2004)* unpublished) and show that the magnetoconductance features can be reproduced if we use a recently developed model that includes decoherence with a phenomenological statistical description. Otherwise, simulations based on completely coherent transport would provide a much richer structure of magnetoconductance, that in experiments is smoothed out by dephasing processes. In particular, we recover experimental features of the magnetoconductance such as magnetic focusing and Shubnikov–de Haas oscillations. By computing the local partial density of states of the system at different values of the external field we recover the semiclassical orbits.

(Some figures in this article are in colour only in the electronic version)

1. Introduction

Mesoscopic devices such as ballistic cavities deal with physical phenomena governed both by quantum mechanical mechanisms, such as interference due to the phase coherent propagation of the wavefunction, and by semiclassical mechanisms, when a large number of conducting channels contribute to transport.

Weak localization (WL) originating from enhanced backscattering and Shubnikov–de Haas (SdH) oscillations of the magnetoconductance originating from magnetic quantization of energy levels belong to the first category [2, 3]. Magnetic focusing (MF) due to commensurability between the classical cyclotron orbit r_c and the cavity length belongs to the latter [4–6]. Such conductance modulations are usually controlled by varying the carrier density through gate voltages or by varying the externally applied magnetic field.

In the ballistic transport regime, and when the temperature is of the order of few tens of mK, so that temperature smearing is negligible, other resonance phenomena such as multiple reflections in the cavity may occur, that lead to rapid and wide oscillations of the conductance when a gate voltage or the magnetic field are swept, so that other conductance modulations are not visible anymore.

Luckily, in experiments it often occurs that only magnetic focusing and SdH oscillations are observed, since they are more robust to the effects of decoherence due to interaction with the environment [4, 7, 8]. Therefore, from the simulation point of view, we can observe MF and SdH oscillations if we are able to introduce a finite degree of dephasing in the transport mechanism.

In this paper we present numerical simulations of magnetotransport in a ballistic cavity obtained by transversally shifting the central section of a quantum wire defined on an SiGe heterostructure and hence generating two constrictions

[3] Present address: CEA-LETI—17 rue des Martyrs 38054 Grenoble, France.

behaving as quantum point contacts. Such a structure has been experimentally fabricated and characterized as described in [1, 9]. We obtain the 2D confining potential by computing the first subband profile from a self-consistent solution of the 3D Schrödinger–Poisson equation on the whole structure and compute the magnetoconductance and the local partial density of states with a code based on the computation of the scattering matrix of the system. The effect of dephasing on the transport properties is included with a statistical treatment of the dephasing process described in a recent work [10]. We are able to recover MF and SdH oscillations of the magnetoconductance as well as semiclassical orbits of carriers inside the cavity. The local partial density of states in the structure can be used to investigate the occurrence of internal orbits which resemble classical motion [8, 6].

The paper is organized as follows. In section 2 we present the methods used to compute the electrostatic and transport properties of the structure in the case in which a coherent transport regime is considered. In section 3 we briefly describe the statistical model for dephasing. Results obtained for a strained Si–SiGe ballistic cavity in the cases of both coherent and partially incoherent transport regimes are presented.

2. Physical model

In this section we consider the physical models used to simulate the transport properties of the SiGe ballistic cavity. First, in order to solve the many body Schrödinger equation with the mean field approximation in a realistic structure, we solve the nonlinear Poisson equation in three dimensions:

$$\nabla [\epsilon(\mathbf{r})\nabla\phi(\mathbf{r})] = -q[p(\mathbf{r}) - n(\mathbf{r}) + N_{\mathrm{D}}^{+}(\mathbf{r}) - N_{\mathrm{A}}^{-}(\mathbf{r}) + \rho_{\mathrm{fix}}], \tag{1}$$

where ϕ is the electrostatic potential, ϵ is the dielectric constant, p and n are the hole and electron densities, respectively, N_{D}^{+} is the concentration of ionized donors, N_{A}^{-} is the concentration of ionized acceptors and ρ_{fix} is the fixed charge density.

The electron density in strongly confined regions is computed by solving the Schrödinger equation with density functional theory in the local density approximation [11–13]. The hole density and the electron density in other regions are computed with the semiclassical expression. The Schrödinger equation for Kohn–Sham single electron states reads

$$-\frac{\hbar^2}{2}\nabla[m^{-1}(\mathbf{r})\nabla\Psi(\mathbf{r})] + \mathrm{V}(\mathbf{r})\Psi(\mathbf{r}) = E\Psi(\mathbf{r}), \tag{2}$$

where $\hbar$ is the reduced Planck's constant, m is the effective mass tensor, and Ψ and E are the eigenfunctions and the eigenvalues, respectively. The confining potential V can be expressed as $V = E_{\mathrm{c}} + V_{\mathrm{exc}}$, where E_{c} is the conduction band edge and V_{exc} is the exchange–correlation potential [14]:

$$V_{\mathrm{exc}} = -\frac{q^2}{4\pi^2\varepsilon_0\varepsilon_r}\left[3\pi^3 n(\mathbf{r})\right]^{\frac{1}{3}}. \tag{3}$$

The coupled Poisson and Schrödinger equations are solved by means of a multigrid algorithm [15]. The Schrödinger equation is solved at the finest grid of each V-cycle along the vertical direction where quantum confinement is present. In the strained silicon channel the 1D Schrödinger equation is solved three times, one for each pair of minima of the silicon conduction band. Once we obtain band and density profiles at quasi-equilibrium, we can compute the transport properties of the device. In the following, the same band profile obtained at zero magnetic field is used to compute all the points of the magnetoconductance curve, assuming negligible corrections to the potential due to the change of the external magnetic field. In this way, the computational resources required are still tractable.

We obtain the quantum conductance G at zero temperature using the Landauer–Büttiker formula [16, 17] that expresses G as a function of the transmission matrix t. The conductance of a generic device depends on the transmission probability matrix $T = tt^{\dagger}$ through the formula

$$G = g\frac{e^2}{h}\sum_n T_n, \tag{4}$$

where g is the degeneracy factor ($g = 4$ in our case due to both spin and valley degeneracy) and the sum is over the all the eigenvalues T_n of the transmission probability operator T. The numerical method is based on the computation of the scattering matrix of the conductor. First, the domain is subdivided into several slices along the propagation direction. For each slice j one can easily compute the scattering matrix S_j by solving the 2D Schrödinger equation with Dirichlet boundary conditions on the transversal cross section and by enforcing continuity of the wavefunction and of the probability current density between adjacent slices. S_j has the form

$$S_j = \begin{pmatrix} r_j & t'_j \\ t_j & r'_j \end{pmatrix}, \tag{5}$$

where t_j (t'_j), and r_j (r'_j) are the transmission and reflection matrices, respectively, from left to right (right to left). In order to compute the total scattering matrix S_{T}, it is sufficient to compose all the S_j matrices [3].

Finally, the presence of a magnetic field $\mathbf{B} = B\hat{\mathbf{z}}$ perpendicular to the propagation plane xy is taken into account by adopting the transverse gauge $\mathbf{A} = Bx\hat{\mathbf{y}} = A(x)\hat{\mathbf{y}}$ for the vector potential $\mathbf{A} = \boldsymbol{\nabla} \times \mathbf{B}$. The new Hamiltonian can be written as the sum of two terms: $H(x, y) = H_{\mathrm{trans}}(y) + H_{\mathrm{long}}(x)$, where $H_{\mathrm{trans}} = [p_y - eA(x_j)]^2/2m_y + V(y)$ refers to the transversal part of the Hamiltonian and $H_{\mathrm{long}} = p_x^2/2m_x$ to the longitudinal one. The eigenvectors are given by the product of the eigenvectors for the two Hamiltonians, that are plane waves for H_{long} and

$$\chi_{n,j}(y) = \chi_{n,j}^{0}(y)\exp[-\mathrm{i}eA(x_j)y/\hbar] \tag{6}$$

for H_{trans}, where $\chi_{n,j}^{0}(x)$ are the solutions in the case $B = 0$. Furthermore, with this gauge, the eigenvalues $E_{j,n}$ are not altered by the presence of the magnetic field. We note that the condition for the validity of the discretization of H_{trans} is that the magnetic flux through a generic slice $[A(x_{j+1}) - A(x_j)]W$ is much smaller than the quantum unit of flux h/e, where W is the transverse device length [18].

3. Dephasing model

In this section we briefly describe a phenomenological approach for including dephasing in the simulation of

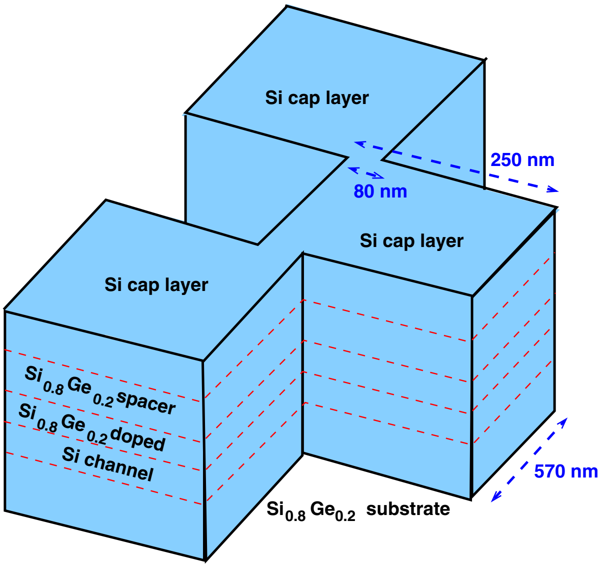

Figure 1. Quantum cavity obtained from a quantum wire defined by etching on an SiGe heterostructure. Dimensions refer to the structure considered in the simulations.

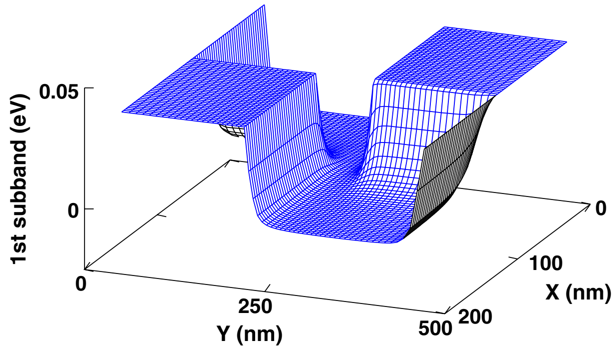

Figure 2. Profile of the first subband for electrons in the vicinity of one constriction.

mesoscopic devices based on the scattering matrix technique. Such a method treats decoherence as a random fluctuation of the phase of the propagating modes involved in the computation of the scattering matrix, and enables us to obtain average conductances and noise spectra from a sufficiently large ensemble of Monte Carlo simulations. A detailed description of the method can be found in [10].

Usually, ballistic transport in mesoscopic structures is addressed in the framework of the Landauer–Büttiker theory of transport, [16, 17] which does not allow for including directly the effects of dephasing. Such effects are normally treated with phenomenological models, based on the insertion of a virtual voltage probe [19] into the ballistic region: electrons travelling from source to drain can be absorbed by the third probe, where they lose their phase information before being re-injected into the conductor. Alternatively, the effect of dephasing can be modelled by adding an imaginary potential to the Hamiltonian in the device region [20, 21], which acts as an absorber of the wavefunction, and introducing an adequate mechanism for the re-injection of phase-randomized particles, in order to ensure continuity of the total current probability density.

Our technique is based on a phenomenological microscopic model, which captures the effect of elastic interactions in terms of a random term added to the phase of the single particle wavefunction. Given the random character of scattering events, each Monte Carlo run provides a particular occurrence of the reduced single particle scattering matrix. Average transport properties are obtained from large samples of Monte Carlo runs.

We introduce in our description the effects of decoherence as a dephasing of the wavefunction. The scattering matrix S_j of the jth slice can be seen as the composition of two submatrices: one takes into account the interface between adjacent slices, and the other takes into account coherent propagation in the slice. Such a latter S-matrix has zero reflection matrices and diagonal transmission matrices, whose mth element is $e^{ik_{j,m}d_j}$ where $d_j = x_{j+1} - x_j$ and $k_{j,m}$ is the wavevector of the mth mode in the jth slice. We modify each element by adding a random phase ϕ_R so that the generic diagonal element of the transmission matrix is $e^{i(k_{j,m}d_j+\phi_R)}$ and ϕ_R is extracted by a random number generator and obeys a zero average Gaussian distribution with variance $\sigma_j^2 = d_j/l_\phi$.

The total scattering matrix obtained in such a way only represents a particular occurrence of the reduced scattering matrix of the single particle. The average reduced scattering matrix is obtained by averaging the conductance over a sufficient number of runs, typically of the order of one hundred. In this way we take into account the intrinsic statistical character of the dephasing process. We emphasize that the usual properties of the scattering matrix S, such as unitarity $SS^\dagger = I$ and the Onsager–Casimir relations [22] for the reciprocity relations of the scattering matrix, still hold [10].

Further, we note that the model can be easily generalized whenever a tight-binding representation of the Hamiltonian is used to compute the transmission probability with recursive Green's function methods and that can be used to study the full current statistics of the structure allowing for addressing the effects of dephasing also on the shot noise and higher cumulants of the current [23].

4. Magnetoconductance of SiGe cavities

We now present results from our simulations of the considered cavity. The structure is depicted in figure 1 and consists of an SiGe heterostructure with the same layer structure described in [9]. Quantum confinement is present along the growth direction and a 2D electron gas is located in the strained-Si channel.

A quantum wire with a width of 250 nm is considered and a section of a length of 570 nm is laterally shifted in order to form a cavity separated from the leads by two quantum constrictions. The two constrictions have a geometrical width of 80 nm, and a much smaller electrical width, as shown in figure 2, where the lowest 2D subband for electrons near one constriction is shown, as obtained from the 3D Poisson–Schrödinger solver. The mesh size used varies from 0.5 to 2 nm along the longitudinal direction (x-axis) and is fixed to 2.5 nm along the y-axis.

The magnetoconductance obtained by Scappucci *et al* [1] presents at 50 mK three magnetic focusing oscillations with conductance peaks at $B = 0.1$, 0.25, and 0.43 T, and minima for $B = 0.17$, and 0.33 T. For higher magnetic field, SdH oscillations appear, whose frequency allows us to extract an

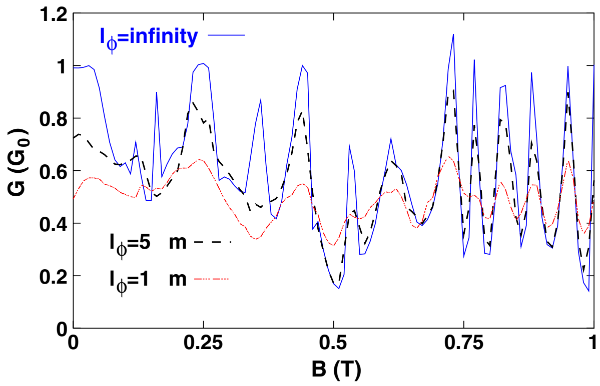

Figure 3. Magnetoconductance of the device shown in figure 1. The solid (blue) curve corresponds to the case $l_\phi \to \infty$, the dashed (black) curve corresponds to the case $l_\phi = 5\ \mu$m, and the dot–dashed (red) curve corresponds to the case $l_\phi = 1\ \mu$m.

electron density of about 7×10^{11} cm^{-2}. From such a value of the electron density we can infer that only one mode propagates through each constriction.

In figure 3 we show the magnetoconductance of the cavity for a Fermi energy of $E_F = 3$ meV, corresponding to only one propagating mode through the constriction. We plot the coherent case (solid curve, $l_\phi \to \infty$), the case $l_\phi = 5\ \mu$m (dashed curve), and $l_\phi = 1\ \mu$m (dash–dotted curve). The partially coherent cases are obtained from a Monte Carlo simulation on an ensemble of 300 runs as described in section 3. Let us stress the fact that resonances due to multiple reflections in the cavity are destroyed by the effect of decoherence. Such resonances are not present in the coherent calculations at high magnetic field, when transport occurs through edge channels. The second effect of the decoherence is to reduce the amplitude of tunable resonances due to MF and SdH oscillations.

The first three maxima of the magnetoconductance are obtained for $B = 0.04$, 0.23, 0.43 T, minima appear for $B = 0.12$, 0.35 T. The agreement with the experiment is very good, also considering the fact that the geometry of the simulated structure only approximates the actual geometry.

Finally, in figure 4 we show the colour plot of the local partial density of states of the system for three specific values of the magnetic field corresponding to two MF peaks in the magnetoconductance plot (states injected from the left) and one minimum. The local density of states $\rho(x_i, y_j, E) = |\Psi(x_i, y_j, E)|^2$ is computed by calculating the wavefunction of the system at each point (x_i, y_j) of the grid with a recursive scattering matrix method. It is interesting to verify that for $B = 0.23$ and 0.43 T we are able to appreciate the pattern of the semiclassical orbit. For $B = 0.23$ T we have $L \sim r_c$, and for $B = 0.43$ T we have $L \sim 2r_c$. For $B = 0.35$ T, corresponding to a conductance minimum, the local density of states reveals very complicate trajectories.

5. Conclusion

In this paper we have presented a numerical simulation of the transport properties of a strained Si–SiGe ballistic cavity. In particular we studied the effects of environmental dephasing in attenuating the oscillation amplitudes and in cancelling dense resonances due to multiple scattering inside the cavity.

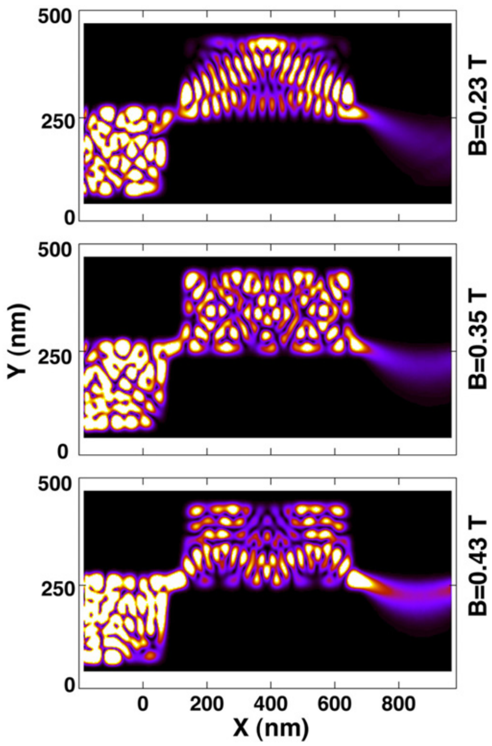

Figure 4. Local partial density of states in the silicon ballistic cavity (states injected from the left) for $B = 0.23$ T (top), $B = 0.35$ T (centre), and $B = 0.43$ T (bottom).

We were able to destroy such uncontrolled resonances and to preserve magnetoconductance oscillations by choosing a degree of decoherence with a coherence length slightly larger than the structure length. Moreover, we presented simulations of the density of states of the system when the applied magnetic field is such that the cyclotron radius is commensurable with the size of the cavity or with a sub-multiple and recover patterns of semiclassical orbits, ensuring the semiclassical origin of such resonances.

Acknowledgments

Partial support from the Italian Ministry for University and Research through the FIRB Project 'Nanotechnologies and nanodevices for the Information Society' and from the EU through the SINANO Network of Excellence (contract no. 506844) is gratefully acknowledged. The authors acknowledge fruitful discussions with G Scappucci and F Evangelisti.

References

[1] Scappucci G *et al* 2004 *Trends in Nanotechnology (Segovia, Spain, Sept. 2004)* unpublished

[2] Ferry D K and Goodnick S M 1997 *Transport in Nanostructures* (Cambridge: Cambridge University Press)

[3] Datta S 1995 *Electronic Transport in Mesoscopic Systems* (Cambridge: Cambridge University Press)

[4] Marcus C M, Rimberg A J, Westervelt R M, Hopkins P F and Gossard A C 1992 *Phys. Rev. Lett.* **69** 506–9

[5] Ye P D and Tarucha S 1999 *Phys. Rev.* B **59** 9794–7

[6] Crook R, Smith C G, Graham A C, Farrer I, Beere H E and Ritchie D A 2003 *Phys. Rev. Lett.* **91** 246803

[7] Bird J P, Ishibashi K, Ferry D K, Ochiai Y, Aoyagi Y and Sugano T 1995 *Phys. Rev.* B **52** 8295–304
[8] Akis R, Ferry D K and Bird J P 1996 *Phys. Rev.* B **54** 17705–15
[9] Notargiacomo A, Di Gaspare L, Scappucci G, Mariottini G, Evangelisti F, Giovine E and Leoni R 2003 *Appl. Phys. Lett.* **83** 302–4
[10] Pala M G and Iannaccone G 2004 *Phys. Rev.* B **69** 235304
[11] Hohenber H and Kohn W 1964 *Phys. Rev.* **136** B864–73
[12] Kohn W and Sham L J 1965 *Phys. Rev.* **140** A1133–8
[13] von Barth U and Hedin L 1972 *J. Phys. C: Solid State Phys.* **5** 1629–42
[14] Inkson J C 1984 *Many Body Theory of Solids—An Introduction* (New York: Plenum)
[15] Iannaccone G, Macucci M, Coli P, Curatola G, Fiori G, Gattobigio M and Pala M 2001 *1st IEEE Conf. on Nanotechnology (Maui, Hawaii, USA, 2001)* (Piscataway, NJ: IEEE) pp 211–6
[16] Landauer R 1957 *IBM J. Res. Dev.* **1** 223
[17] Büttiker M 1988 *IBM J. Res. Dev.* **32** 306
[18] Governale M and Boese D 2000 *Appl. Phys. Lett.* **77** 3215–7
[19] Büttiker M 1986 *Phys. Rev.* B **33** 3020–6
[20] Czycholl G and Kramer B 1979 *Solid State Commun.* **32** 945
[21] Efetov K B 1995 *Phys. Rev. Lett.* **74** 2299–302
[22] Onsager L 1931 *Phys. Rev.* **38** 2265–79
Casimir H B G 1945 *Rev. Mod. Phys.* **17** 343–50
[23] Pala M G and Iannaccone G 2004 *Phys. Rev. Lett.* **93** 256803